High-Resolution Mapping of the Spatial Organization of a Bacterial Chromosome

Tung B. K. Le,[1] Maxim V. Imakaev,[2] Leonid A. Mirny,[2,3]* Michael T. Laub[1,4]*

Chromosomes must be highly compacted and organized within cells, but how this is achieved in vivo remains poorly understood. We report the use of chromosome conformation capture coupled with deep sequencing (Hi-C) to map the structure of bacterial chromosomes. Analysis of Hi-C data and polymer modeling indicates that the *Caulobacter crescentus* chromosome consists of multiple, largely independent spatial domains that are probably composed of supercoiled plectonemes arrayed into a bottle brush–like fiber. These domains are stable throughout the cell cycle and are reestablished concomitantly with DNA replication. We provide evidence that domain boundaries are established by highly expressed genes and the formation of plectoneme-free regions, whereas the histone-like protein HU and SMC (structural maintenance of chromosomes) promote short-range compaction and the colinearity of chromosomal arms, respectively. Collectively, our results reveal general principles for the organization and structure of chromosomes in vivo.

In all organisms, chromosomal DNA must be compacted by nearly three orders of magnitude to fit within the limited volume of a cell. Chromosomes must adopt structures that are compatible with critical cellular processes such as transcription, DNA replication, and chromosome segregation. Although bacterial chromosomes are probably highly organized within cells (*1*–*6*), the resolution of previous studies has been limited. For eukaryotes, chromosome conformation capture coupled with deep sequencing, or Hi-C, has enabled higher-resolution studies of chromosome structure in vivo (*7*, *8*). These studies have suggested that interphase chromosomes are organized into a series of topological or structural domains <1 Mb in size (*8*–*11*), but the factors that create, maintain, and influence these domains are presently unknown.

To study the organization of bacterial chromosomes with high resolution, we used Hi-C on *Caulobacter* cells (figs. S1 and S2). We performed Hi-C on swarmer cells that each contain a single circular and unreplicated chromosome. To analyze our Hi-C data, we divided the genome into 10-kilobase (kb) bins, with interaction frequencies for each restriction fragment assigned to corresponding bins. We visualized interactions as a heat map where each matrix position, m_{ij}, reflects the relative frequency of interactions be-

[1]Department of Biology, Massachusetts Institute of Technology (MIT), Cambridge, MA 02139, USA. [2]Department of Physics, MIT, Cambridge, MA 02139, USA. [3]Institute for Medical Engineering and Sciences, MIT, Cambridge, MA 02139, USA. [4]Howard Hughes Medical Institute, MIT, Cambridge, MA 02139, USA.

*Corresponding author. E-mail: laub@mit.edu (M.T.L.); leonid@mit.edu (L.A.M.)

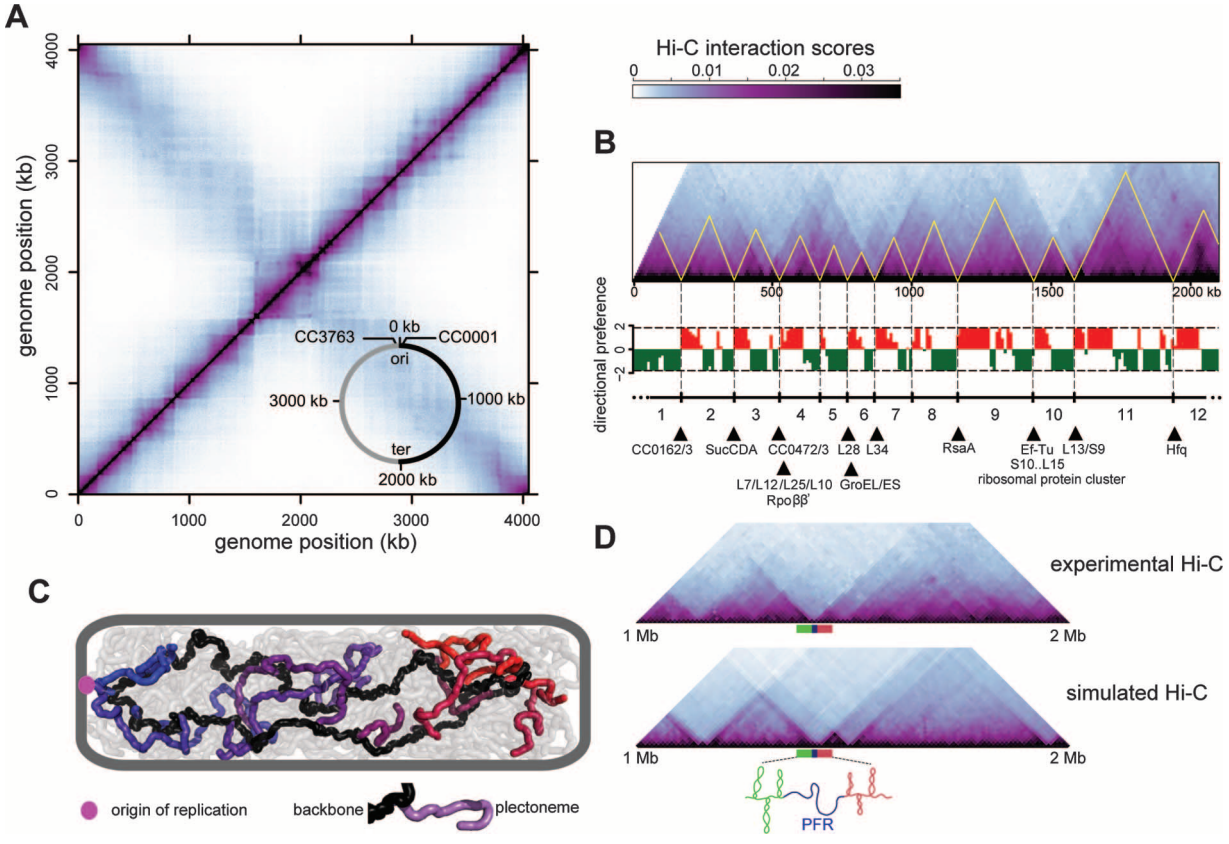

Fig. 1. Partitioning of the *Caulobacter* chromosome into CIDs. (**A**) Normalized NcoI Hi-C contact map for *Caulobacter* swarmer cells displaying contact frequencies for pairs of 10-kb bins across the genome. Axes indicate the genome position of each bin. (Inset) Simplified genomic map showing the origin of replication (*ori*) and terminus (*ter*), along with the right (black) and left (gray) chromosomal arms. (**B**) Hi-C contact map for one arm of the chromosome rotated 45° clockwise with directional preference plots below. Left- and rightward preferences are shown as green and red bars, respectively. CIDs are outlined in yellow and numbered. Highly expressed genes at CID boundaries are listed (hypothetical genes are designated by GenBank ID no.). (**C**) Polymer chromosome model showing the polarly anchored origin (magenta), chromosome backbone (black), and plectonemes (gray, with every 10th plectoneme on one arm in a color). (**D**) Comparison of experimental and simulated Hi-C contact maps, indicating that PFRs can account for CIDs.

tween loci in bins *i* and *j*. For a description of data processing, normalization, reproducibility, and comparability to a previous 5C study (*4*), see the supplementary materials (figs. S3 to S6).

The swarmer cell interaction matrix contains two prominent diagonals (Fig. 1A). The main diagonal reflects high-frequency interactions between loci on the same chromosomal arm. The other, less prominent diagonal captures lower-frequency inter-arm contacts; i.e., those between loci on one chromosomal arm and those on the opposite arm of the circular genome. These locus pairs are separated by substantial distances in the primary genome sequence, but the Hi-C data indicate that they are often physically adjacent and capable of interacting. This overall pattern, also seen with 5C data (*4*), is consistent with the *Caulobacter* chromosome adopting an elongated structure, with the single origin anchored at one pole and the two chromosome arms running the length of the cell in close proximity.

Further inspection of the Hi-C interaction matrix revealed highly self-interacting regions, or chromosomal interaction domains (CIDs), of the genome that appear as squares along the main diagonal (Fig. 1A) or as triangles if the contact map is rotated 45° clockwise (Fig. 1B and figs. S7 and S8). Loci within a CID interact preferentially with other loci within the same CID as compared to other CIDs. Loci at the border of each CID strongly favor interactions with loci on their left- or righthand side, but not both, whereas loci in the middle of a CID show high levels of interaction with loci on both sides. The Hi-C matrix exhibited variability in boundary sharpness and some nested domains (Fig. 1B and figs. S8 and S9). This hierarchical organization resembles the so-called topologically associated domains (TADs) previously observed in eukaryotic Hi-C data (*8*–*11*).

To systematically map the boundaries of CIDs, we generated plots of directional preference as a function of genome position (Fig. 1B and figs. S7 to S9). There were 23 CIDs, ranging in length from 30 to 420 kb (table S1). CIDs were not artefacts of restriction site or sequencing-read densities (fig. S10) and were independently verified with a recombination-based assay for interaction frequencies (fig. S11). The CIDs identified must be present in most cells, because Hi-C reflects interactions in a population of cells. Individual cells could have other, perhaps transient, domains.

CID boundaries were enriched in highly expressed genes ($P = 7.7 \times 10^{-5}$, Fisher's exact test, fig. S10). Of the 23 CID boundaries, 17 contained one or more highly transcribed genes (Fig. 1B and figs. S8 and S10). We hypothesized that high gene expression unwinds the DNA duplex and creates plectoneme-free regions (PFRs), which form barriers between CIDs. These PFRs probably prevent the diffusion of supercoils and physically separate CIDs, thereby decreasing the contact probabilities of loci in different domains, as also suggested in *Salmonella* (*1*).

To better understand the three-dimensional organization of the *Caulobacter* chromosome, we developed a detailed polymer model (figs. S12 to S15). The chromosome was modeled as a circular polymer comprising a dense array of plectonemes that have no sequence specificity and are stochastic in length and location (Fig. 1C and fig. S12). We generated an equilibrium ensemble of chromosome conformations, simulated the Hi-C procedure on 25,000 modeled chromosomes, and compared the resulting data to experimental Hi-C data. By systematically varying model parameters, we identified values that provided the best fit to the observed Hi-C contact frequencies (figs. S13 and S14).

Our model reflects two broad levels of chromosomal organization. On one level, the DNA is arranged into a fiber of ~300 plectonemes separated by small spacers, resembling a bottle brush. Plectonemes ~15 kb in length separated by less than 300 bp provided the best agreement to Hi-C data. At a higher level, the bottle brush fiber forms a circular chromosome tethered at the pole by an origin-proximal region with chromosomal arms in close proximity down the long axis of the cell. We also used the model to examine the effects of PFRs on interactions between loci. A single PFR of ~2 kb created a space of ~100 to 200 nm between flanking loci. This spacer reduced contacts between neighboring plectonemes and prevented the diffusion of supercoils through the PFR in the simulations, recapitulating a CID boundary (Fig. 1D and fig. S16). We then introduced PFRs into the chromosome model at the locations of the 20 most highly expressed genes. Simulated Hi-C data generated a pattern of CIDs that resembled those observed experimentally, supporting the hypothesis that PFRs can induce CIDs (Fig. 1D and fig. S17).

To probe the role of gene expression in chromosome structure, we performed Hi-C on swarmer cells treated for 30 min with rifampicin (rif), an inhibitor of transcription elongation (*12*). The interaction matrix of rif-treated cells was globally similar to that of untreated cells, indicating that the overall shape of the chromosome was unperturbed (Fig. 2, A and B). However, CID boundaries were severely disrupted in rif-treated cells, leading to a nearly domain-free organization (Fig. 2B and figs. S18 and S19). Simulations of rif-treated chromosomes, performed by removing PFRs, also produced domain-free contact maps (figs. S19 to S21).

We also moved the highly expressed gene *rsaA* to the *vanA* locus, a poorly expressed region of the genome (fig. S22). The native *vanA* locus normally resides within a CID, but the insertion of *rsaA* generated a sharp new CID boundary at this position in the genome (Fig. 2C). Relocating *rsaA* to the *xylX* locus, ~1.7 Mb from the *vanA* locus, also created a new CID boundary at this location (fig. S23). We conclude that highly expressed genes play a direct role in defining chromosomal domain boundaries.

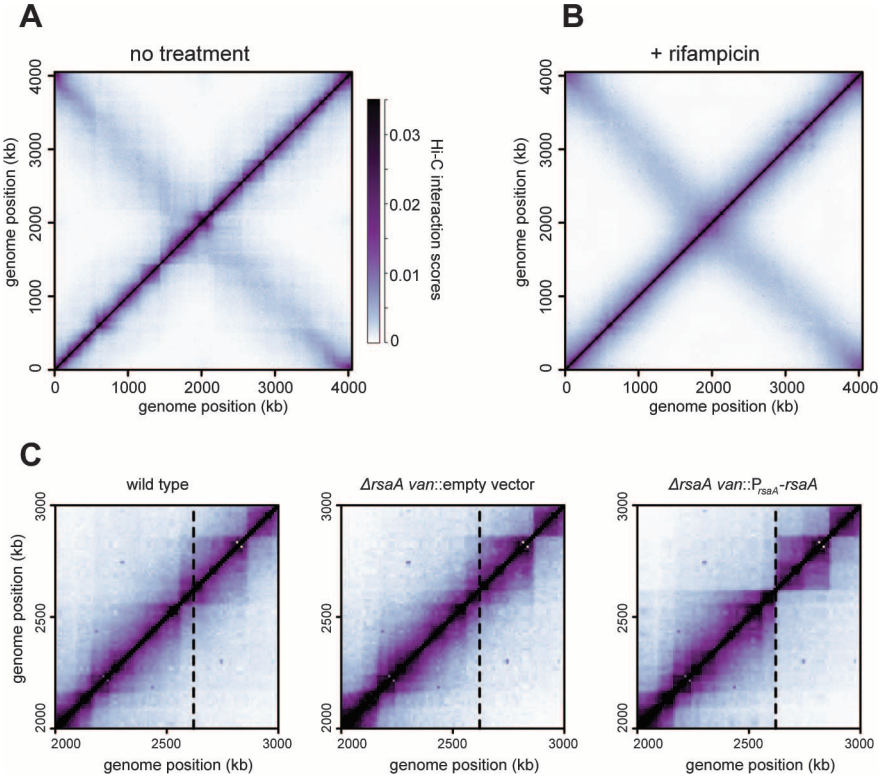

Fig. 2. Effect of inhibiting transcription on CID boundaries. Normalized BglII Hi-C contact maps for (**A**) untreated and (**B**) rif-treated swarmer cells. (**C**) Hi-C contact maps for wild-type, Δ*rsaA*, and Δ*rsaA* + *van*::P_{rsaA}-*rsaA* cells. Only the region of the genome containing the *van* locus (dashed line) is shown.

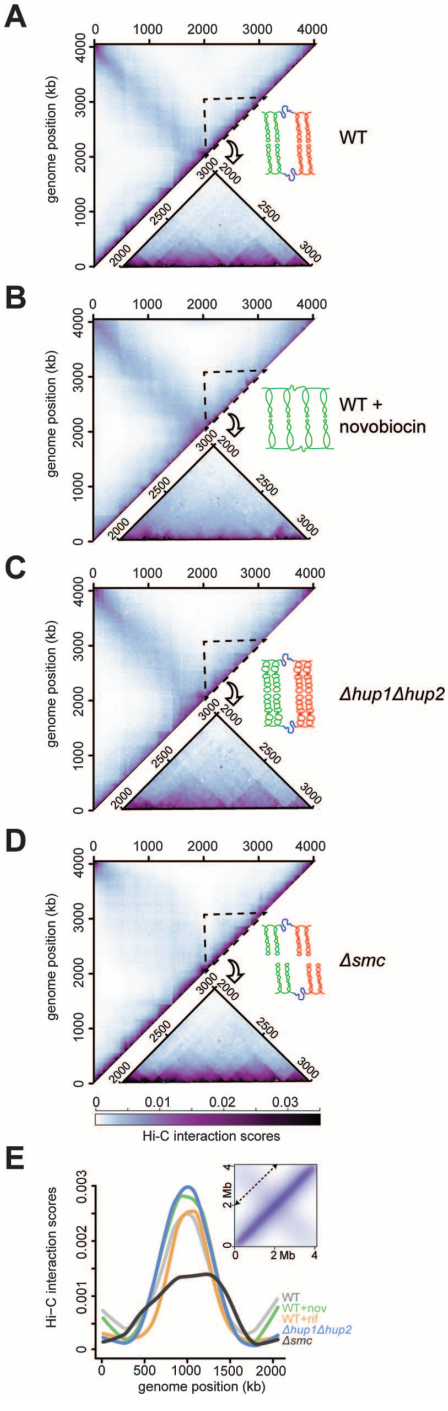

Fig. 3. Contribution of supercoiling, HU, and SMC to chromosome organization. Normalized BglII Hi-C contact maps for (**A**) wild-type, (**B**) novobiocin-treated wild-type, (**C**) Δ*hup1*Δ*hup2*, and (**D**) Δ*smc* swarmer cells. Only the upper left regions of the symmetric Hi-C maps are shown. A region from 2 to 3 Mb is enlarged and shown below each map. A cartoon summarizing the effects of each perturbation is shown, with neighboring domains of plectonemic DNA in red and green and plectoneme-free regions in blue. (**E**) Hi-C scores for the diagonal (indicated in the inset) of each contact map.

We also used Hi-C to probe the effect of inhibiting supercoiling on chromosomal organization. Swarmer cells were incubated for 30 min with a sublethal dose of novobiocin (fig. S24) and then subjected to Hi-C analysis (Fig. 3, A and B, and fig. S18). Novobiocin, which inhibits DNA gyrase and negative supercoiling (*13*), significantly reduced the frequency of interactions in the 20- to 200-kb range while modestly increasing interactions in the 200- to 800-kb range relative to the untreated wild type (fig. S25). Additionally, novobiocin reduced the sharpness and positions of CID boundaries (Fig. 3B and fig. S18). The decrease in interaction frequencies in the 20- to 200-kb range does not result from the emergence of a subpopulation of cells with gross defects in chromosome organization (fig. S26).

To model the effect of novobiocin, we increased the spacing between duplexes in a plectoneme monomer and increased the average spacing between plectonemes fivefold. Subsequent simulations reproduced the partial loss of CID boundaries and changes in contact frequencies observed (figs. S19, S20, and S27). Taken together, our results demonstrate that supercoiling is (i) critical to genome compaction in the 20- to 200-kb range and (ii) helps establish CIDs in vivo.

To investigate the role of nucleoid-associated proteins in chromosomal organization, we focused on the histone-like proteins HU1 and HU2 (*14*, *15*). We isolated swarmer cells from a Δ*hup1*Δ*hup2* strain and performed Hi-C. The interaction matrix for Δ*hup1*Δ*hup2* was grossly similar to that of wild-type cells (Fig. 3C). The correlation between directional preferences for each bin along the chromosome of wild-type and Δ*hup1*Δ*hup2* cells was high ($r = 0.73$, $P < 10^{-15}$), indicating that CID boundaries were retained, although they became less pronounced in the absence of HU1 and HU2 (fig. S28). The contact probability plot for Δ*hup1*Δ*hup2* cells revealed a significant decrease in short-range contacts, up to ~100 kb, compared to the wild type (fig. S25). These changes suggest that deleting HU may disrupt interactions within and between neighboring plectonemes without affecting interplectoneme spacing, which is critical for producing CID boundaries (Fig. 3C and fig. S20). We modeled the effect of deleting HU by increasing the spacing between duplexes within a plectoneme; simulations based on this model recapitulated the Hi-C data (fig. S29). These analyses indicate that HU facilitates local short-range compaction of the genome, possibly through the packing and stabilization of plectonemic DNA.

SMC (structural maintenance of chromosomes) homologs are found in all domains of life and can form ringlike structures that facilitate chromosome cohesion or compaction (*16*–*18*). Hi-C analysis of *Caulobacter* Δ*smc* swarmer cells showed a clear drop in the frequency of interchromosomal arm interactions (Fig. 3, D and E). Concomitantly, loci typically interacted with a wider range of loci on the opposite chromosomal arm than did wild-type cells. In contrast, the frequencies of intra-arm interactions (fig. S25) and CID boundaries (fig. S28) were largely unaffected in the absence of SMC. Although many bacterial SMC proteins may compact DNA (*19*, *20*), our data suggest that *Caulobacter* SMC contributes primarily to the colinearity of chromosome arms in swarmer cells.

To study chromosome organization changes during cell cycle progression, we performed Hi-C on synchronized cells collected at regular intervals during the cell cycle (Fig. 4). After replication initiation in *Caulobacter*, one origin remains near the stalked pole while the other

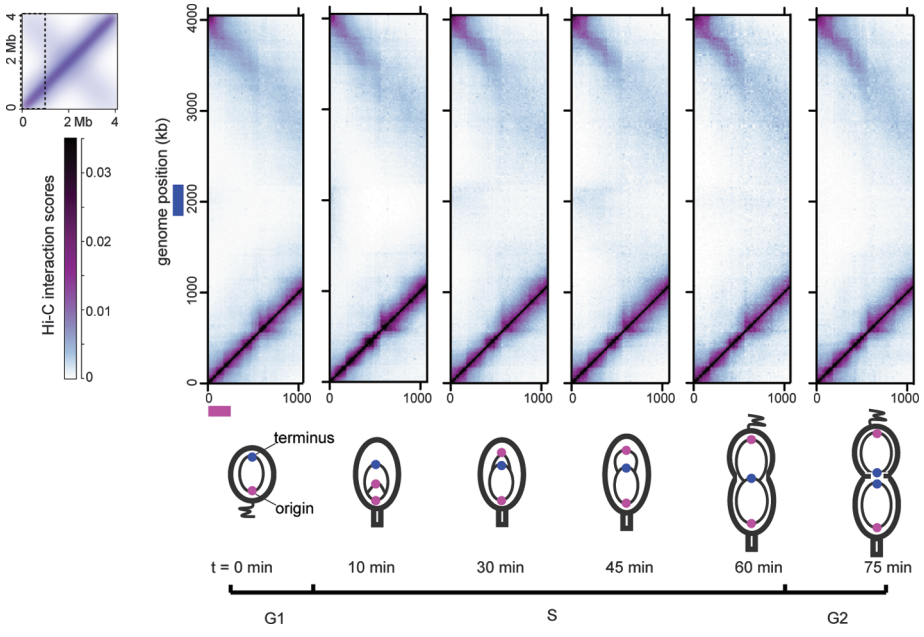

Fig. 4. Dynamics of chromosomal organization during cell cycle progression. Plots show a section of the Hi-C interaction map for the cell cycle time points indicated.

moves to the opposite pole (*6*). As the cell cycle progressed, the Hi-C contact maps indicated progressively more interactions between origin- and terminus-proximal loci (Fig. 4 and fig. S30), particularly at the 30- and 45-min time points, when the newly translocated origin is close to the polarly localized terminus (Fig. 4). However, the frequency of these interactions was still nearly 16-fold less than an average interaction between loci within 100 kb. This difference implies that the translocating chromosome is largely insulated from the anchored chromosome despite their physical proximity, which is likely to be advantageous to the segregation process by preventing the entanglement of chromosomes destined for different daughter cells. Also, the CIDs identified in swarmer cells (Fig. 1, A and B) remained intact throughout the cell cycle (Fig. 4), indicating that CIDs must get reestablished concurrently with, or shortly after, DNA replication (figs. S31 and S32), which may also help keep newly replicated chromosomes from becoming entangled.

CIDs are reminiscent of the TADs documented in eukaryotes (*9*–*11*, *21*), suggesting that domains on a 100-kb length scale are a fundamental unit of chromosome structure in all organisms. Like TADs, *Caulobacter* CIDs often appear as nested domains, which may be related to the megabase-scale macrodomains identified in *Escherichia coli* (*3*, *5*). The identification of CIDs indicates that many domain barriers in *Caulobacter* are relatively fixed; however, within each CID there could be additional barriers that arise and dissipate, perhaps stochastically, as suggested in *Salmonella* and *E. coli* (*1*, *22*), and CID boundaries may change in different growth conditions. Although chromosomal domains have now been documented in several organisms, the factors determining domain boundaries had been unclear. Although the DNA binding proteins HU and SMC contribute to chromosome organization, they do not significantly affect CIDs. Instead, our work points to supercoiling and highly expressed genes as critical determinants of domain formation in bacteria, and we suspect that similar mechanisms contribute to creating TADs in higher organisms, where boundaries may also be enriched in highly expressed genes (*9*).

References and Notes

1. B. M. Booker, S. Deng, N. P. Higgins, *Mol. Microbiol.* **78**, 1348–1364 (2010).
2. J. K. Fisher *et al.*, *Cell* **153**, 882–895 (2013).
3. H. Niki, Y. Yamaichi, S. Hiraga, *Genes Dev.* **14**, 212–223 (2000).
4. M. A. Umbarger *et al.*, *Mol. Cell* **44**, 252–264 (2011).
5. M. Valens, S. Penaud, M. Rossignol, F. Cornet, F. Boccard, *EMBO J.* **23**, 4330–4341 (2004).
6. P. H. Viollier *et al.*, *Proc. Natl. Acad. Sci. U.S.A.* **101**, 9257–9262 (2004).
7. J. Dekker, K. Rippe, M. Dekker, N. Kleckner, *Science* **295**, 1306–1311 (2002).
8. E. Lieberman-Aiden *et al.*, *Science* **326**, 289–293 (2009).
9. J. R. Dixon *et al.*, *Nature* **485**, 376–380 (2012).
10. E. P. Nora *et al.*, *Nature* **485**, 381–385 (2012).
11. T. Sexton *et al.*, *Cell* **148**, 458–472 (2012).
12. E. A. Campbell *et al.*, *Cell* **104**, 901–912 (2001).
13. M. Gellert, M. H. O'Dea, T. Itoh, J. Tomizawa, *Proc. Natl. Acad. Sci. U.S.A.* **73**, 4474–4478 (1976).
14. S. C. Dillon, C. J. Dorman, *Nat. Rev. Microbiol.* **8**, 185–195 (2010).
15. F. Guo, S. Adhya, *Proc. Natl. Acad. Sci. U.S.A.* **104**, 4309–4314 (2007).
16. A. Badrinarayanan, R. Reyes-Lamothe, S. Uphoff, M. C. Leake, D. J. Sherratt, *Science* **338**, 528–531 (2012).
17. T. Hirano, *Nat. Rev. Mol. Cell Biol.* **7**, 311–322 (2006).
18. M. A. Schwartz, L. Shapiro, *Mol. Microbiol.* **82**, 1359–1374 (2011).
19. P. L. Graumann, T. Knust, *Chromosome Res.* **17**, 265–275 (2009).
20. A. Volkov, J. Mascarenhas, C. Andrei-Selmer, H. D. Ulrich, P. L. Graumann, *Mol. Cell. Biol.* **23**, 5638–5650 (2003).
21. C. Hou, L. Li, Z. S. Qin, V. G. Corces, *Mol. Cell* **48**, 471–484 (2012).
22. L. Postow, C. D. Hardy, J. Arsuaga, N. R. Cozzarelli, *Genes Dev.* **18**, 1766–1779 (2004).

Acknowledgments: Hi-C data were deposited in the Gene Expression Omnibus (accession no. GSE45966). We thank M. Umbarger for help in optimizing Hi-C and G. Fudenberg, A. Goloborodko, M. Hu, and T. Maxwell for discussions. M.T.L. is an Early Career Scientist of the Howard Hughes Medical Institute. T.B.K.L is a Gordon and Betty Moore Foundation postdoctoral fellow of the Life Sciences Research Foundation. This work was supported by NIH grants to M.T.L. (R01GM082899) and L.A.M. (U54CA143874).

Supplementary Materials

www.sciencemag.org/content/342/6159/731/suppl/DC1
Materials and Methods
Figs. S1 to S34
Tables S1 to S4
References (*23*–*25*)

17 June 2013; accepted 8 October 2013
Published online 24 October 2013;
10.1126/science.1242059

Mitochondrial Fusion Directs Cardiomyocyte Differentiation via Calcineurin and Notch Signaling

Atsuko Kasahara,[1] Sara Cipolat,[2]* Yun Chen,[3] Gerald W. Dorn II,[3]† Luca Scorrano[2,4]†

Mitochondrial morphology is crucial for tissue homeostasis, but its role in cell differentiation is unclear. We found that mitochondrial fusion was required for proper cardiomyocyte development. Ablation of mitochondrial fusion proteins Mitofusin 1 and 2 in the embryonic mouse heart, or gene-trapping of *Mitofusin 2* or *Optic atrophy 1* in mouse embryonic stem cells (ESCs), arrested mouse heart development and impaired differentiation of ESCs into cardiomyocytes. Gene expression profiling revealed decreased levels of transcription factors transforming growth factor–β/bone morphogenetic protein, serum response factor, GATA4, and myocyte enhancer factor 2, linked to increased Ca^{2+}-dependent calcineurin activity and Notch1 signaling that impaired ESC differentiation. Orchestration of cardiomyocyte differentiation by mitochondrial morphology reveals how mitochondria, Ca^{2+}, and calcineurin interact to regulate Notch1 signaling.

Given their participation in metabolism, signaling, and cell death (*1*), mitochondria are essential for tissue homeostasis. During development, mitochondria control apoptosis and supply adenosine triphosphate (ATP) essential for differentiation (*2*), which is especially important in energy-demanding cells like cardiomyocytes (*3*). Organellar morphology regulates both mitochondrial apoptosis and ATP production: Ablation of the inner mitochondrial membrane mitochondria-shaping protein optic atrophy 1 (OPA1) (*4*) and of the outer mitochondrial membrane mitofusin (MFN)–1 and -2 (*5*) is embryonic lethal, and their conditional deletion in cardiomyocytes causes cardiomyopathy in *Drosophila* (*6*) and in the mouse (*7*, *8*). How mitochondria participate in developmental cascades remains unclear.

We investigated embryonic lethality provoked by cardiomyocyte-restricted, combined *Mfn1* and *Mfn2* ablation (KO) (*8*, *9*). Frequencies of KO embryos between embryonic day 8.5 (E8.5) and E10.5 were only slightly depressed, whereas lethality occurred thereafter (Fig. 1A, fig. S1A, and table S1). At E9.5, hearts of control and KO embryos were nearly indistinguishable, but by E12.5 to E13.5, KO hearts were markedly hypoplastic, with biventricular wall thinning and poor trabeculation (Fig. 1B and figs. S1 and S2). Mitochondria of KO cardiomyocytes were fragmented (fig. S3). Steady-state mRNA expression levels of some central embryonic cardiomyocyte differentiation and proliferation regulators were decreased at E9.5 (Fig. 1C and fig. S4). Accord-

[1]Department of Cell Physiology and Metabolism, University of Geneva, 1206 Geneva, Switzerland. [2]Dulbecco-Telethon Institute, Venetian Institute of Molecular Medicine, 35129 Padova, Italy. [3]Department of Internal Medicine, Center for Pharmacogenomics, Washington University School of Medicine, St. Louis, MO, USA. [4]Department of Biology, University of Padua, 35121 Padova, Italy.

*Present address: Centre for Stem Cells and Regenerative Medicine, King's College London, London SE1 9RT, UK.
†Corresponding author. E-mail: luca.scorrano@unipd.it (L.S.); gdorn@DOM.wustl.edu (G.W.D.)

Editor's Summary

Caulobacter Chromosome

Chromosomal DNA must be highly compacted to fit within the tiny volume of the cell, while at the same time it must maintain a conformation that allows critical cellular processes access to the genome. **Le *et al.*** (p. 731, published online 24 October) analyzed the structure of the circular chromosome in the prokaryote *Caulobacter crescentus* by using chromosome conformation capture and deep-sequencing. Highly self-interacting regions (chromosomal interaction domains, or CIDs) were observed ––similar to the topologically associated domains previously seen in eukaryotes. Supercoiling helped to establish CIDs, and CID boundaries were defined by highly expressed genes. CIDs appeared to be established during or shortly after DNA replication, and could potentially facilitate chromosomal segregation by preventing newly replicated chromosomes from becoming entangled.